Towards sustainable synthesis of polyesters: a QM/MM study of the enzymes CalB and AfEST.

Pedro Figueiredo[‡ξ], Beatriz C. Almeida[‡ξ], Daniel F.A.R. Dourado[§], Andreia F. Sousa[†], Armando J. D. Silvestre[†], Alexandra T. P. Carvalho*[ξ]

[ξ] CNC – Center for Neuroscience and Cell Biology, Institute for Interdisciplinary Research (IIIUC), University of Coimbra, 3004-504 Coimbra (Portugal)

[§] Almac Sciences, Department of Biocatalysis and Isotope Chemistry, Almac House, 20 Seagoe Industrial Estate, Craigavon, BT63 5QD (Northern Ireland UK)

[†] CICECO – Aveiro Institute of Materials, 3810-193 Aveiro (Portugal)

Abstract

Modern society is heavily reliant on synthetic polymers, commonly known as plastics; however plastic pollution is causing an immeasurable damage to marine and land eco-systems. Sustainable alternatives are actively being sought-after, such as biodegradable polyesters obtained by enzymatic synthesis. However, wild type enzymes still pose fundamental efficiency limitations. Protein reengineering approaches can circumvent those building up highly specific, selective and thermostable variants. Here we compare in detail the catalytic mechanisms for poly-caprolactone synthesis by the wild type enzymes *Archaeoglobus fulgidus* carboxylesterase (AfEST) and *Candida antarctica* lipase B (CalB) by performing Quantum mechanics calculations and Quantum Mechanics/Molecular Mechanics Molecular Dynamics simulations. We found that bond forming/breaking events are concerted with proton transfer to or from the catalytic histidine in all the transition states, but with different degrees of coupling between the motions of the atoms involved. Our results give important insights towards the design of new enzyme variants combining good activity with high thermostability in the synthesis of polycaprolactone, which due

24   to its biodegradability, biocompatibility and permeability characteristics is of great importance for biomedical

25   applications, such as protein delivery, tissue engineering, gene delivery, orthopedic devices and resorbable su-

26   tures.

Introduction

28   Synthetic polymers are extensively used by industry and technologies such as in packaging, textiles, electronic

29   devices, machinery, pharmacy and by medicine as highly advanced materials[1]. However, in the last years, ecolog-

30   ical concerns have stimulated the search for better alternatives to commodity plastics, especially because most of

31   these polymers are non-biodegradable, persisting on the environment. There is, thus, a great urgency to find more

32   sustainable alternatives, since plastic pollution is endangering ecosystems[2].

33   Precisely, due to the non-biodegradability of conventional commercial polymers like poly(propylene) and

34   poly(ethylene), the aliphatic-family of polyesters have been on the spotlight due to their ability to biodegrade in a

35   reasonable time-scale[3]. Among aliphatic polyesters, poly(caprolactone) (PCL) deserves a special focus for its bio-

36   degradability, biocompatibility and permeability, meaning that PCL is a good candidate for biomedical applica-

37   tions, such as protein delivery, tissue engineering, gene delivery, orthopedic devices and resorbable sutures[4–7].

38   However, widespread commercialization of PCL is hampered due to synthesis and production issues, together

39   with related economic obstacles, although the thermoplastic supply and demand of biodegradables is on high[8] and

40   PCL could be fueled up.

41   Synthesis of polyesters (e.g. PCL), can be performed mainly by two distinct mechanisms: (i) polycondensation

42   polymerization and (ii) ring-opening polymerization (ROP)[3]. The major drawbacks of polycondensation mecha-

43   nism are the high temperatures and long reaction times generally required, that favor racemization[9], as well as, the

44   systematic use of hazardous metallic catalysts. But in the case of reactions performed by ROP, they can be highly

45   efficient because no byproducts, such as alcohols, are produced and no substrates need to be activated. This is a

46   significant advantage over polycondensation polymerization both from a green chemistry perspective due to the

47   atom-efficiency, but also because yields and molecular weights are favored[10,11]. Aiming to achieve the desired

48   polymer properties, the ROP mechanism has been continuously refined over the years[1]. Several combinations of

49   initiators and catalysts have been evaluated for ROP synthesis, and enzyme-catalyzed ROP was considered one of

50   the most promising approaches[10,12,13]. When compared to conventional chemical routes, enzymatic catalysis gives

2

51   a more precise construction of well-defined structures, such as highly control of enantio-, chemo-, regio-, stereo-

52   and choro-selectivity. More important, enzymes are recyclable, eco-friendly, usually do not require the use of tox-

53   ic reagents, and avoid the problems associated with trace residues of metallic catalysts[11,14].

54   Several lipases (EC 3.1.1.3) and some carboxylesterases (EC 3.1.1.1) have been employed to produce

55   polyesters over different ROP conditions, yielding polymers with a vast array of molecular weights (M_w)[12,15].

56   Among lipases the immobilized lipase B from *Candida antarctica* (CalB) is one of the most studied[15–19]. Alt-

57   hough this enzyme is able to synthesize, in some instances, polyesters with relatively high molecular weights and

58   good yields[20,21] (including PCL), in most cases the polymers have low molecular weights[22,23]. Other factors that

59   limit the industrial application of these enzymes are: (i) the low activity and selectivity for some monomers; (ii)

60   unfavorable compatibility in chemoenzymatic reactions; (iii) low stability under harsh reactions conditions[24]. Re-

61   garding the last point, although CalB immobilization increases the stability and reusability of the enzyme, the

62   immobilized enzyme still displays maximum activity at 40 ºC with substantial activity drop at higher tempera-

63   tures for some substrates[18]. Even when higher catalytic activities are obtained with temperatures in range of 60-

64   80°C, which happens for many substrates and in low-polarity solvents[25], higher molecular weight polymers are

65   frequently produced at lower reaction temperatures (40°C, 45°C)[18,26,27]. Hence, the severe conditions required at

66   industrial scale can compromise catalysis.

67   However, rational protein engineering approaches can be employed to address these limitations and expand the

68   scope of enzymes for polyester synthesis by ROP [28–30]. Particularly good starting points for enzyme design are

69   enzymes from thermophiles, which have been recognized as potential catalysts in various biotechnology applica-

70   tions[31–34]. The thermophilic esterase from the hyper-thermophilic archaeon *Archaeoglobus fulgidus* (AfEST) was

71   previously tested for the synthesis of the aliphatic polyester PCL in various organic solvents and solvent-free sys-

72   tems[35–38]. The free form of the enzyme (at a concentration of 25 mg/ml), catalyzes the formation of polymer

73   chains with number-average molecular weight (M_n) of 1400 g/mol and with a monomer conversion of almost

74   100%, in toluene at 80 ºC for 72h[37]. On the other hand, the immobilized form of the enzyme (80 mg), achieves

75   the production of polymer chains with molecular mass (M_n) of 1160 g/mol and monomer conversion of 100%, in

76   the same conditions[38]. Meaning, that the immobilization process in AfEST does not necessarily produce polymers

77   with higher molecular weights.

78   Considering PCL as case-study for aliphatic polyesters synthesis, here, we draw lessons from how CaLB and

79   AfEST differently achieve PCL synthesis in the quest to obtain enzymes able to match high conversion with high

80   thermostability. We compare in detail, the catalytic mechanisms of the wild type enzymes by performing Quan-

81   tum Mechanics/Molecular Mechanics (QM/MM) Molecular Dynamics (MD) simulations and QM calculations.

82

83   **Methods**

84   **Initial systems setup and classical Molecular Dynamics of the intermediates**

85   The initial structures were modeled from AfEST and CalB crystal structures (pdb codes 1JJI[39] and 5A71[40], re-

86   spectively) and protonation states were assigned with MolProbity[41]. The reactants (**RC**), intermediates (**INT-1**,

87   **EAM** and **INT-2**) and products (**PC**) were geometry optimized in Gaussian09[42] using B3LYP[43], with the 6-

88   31G(d) basis sets and a Polarizable Continuum Model (PCM)[44] solvent description. Atomic partial charges were

89   calculated resorting to the Restrained Electrostatic Potential (RESP)[45] method from HF/6-31G(d) single point en-

90   ergy calculations. The initial position of ε-caprolactone (**ε-Cl**) was obtained by Molecular docking. The MD sim-

91   ulations of all the intermediates in the reaction profiles were performed using the Amber molecular dynamics

92   program (AMBER18)[46] with the parm99SB[47] and GAFF[48] force fields. All the minima in the catalytic cycle were

93   subjected to 20 ns triplicate simulations with different initial velocities, for a total combined time of 60 ns. Refer-

94   ence structures were calculated for all simulations, based on the structure with lowest root-mean-square deviation

95   (RMSD) to the average of the simulation[49]. More information can be found in the Supporting information (SI) -

96   Material and Methods.

97

98   **Quantum mechanical/molecular mechanical (QM/MM) calculations**

99   The QM/MM calculations[50] were performed using the internal semi-empirical hybrid QM/MM functionality

100   implemented in AMBER18[46] with periodic boundary conditions. The PM6[51,52] semi-empirical method was em-

101   ployed for the high-level layer (QM) and the MM region was described by the Amber parm99SB force field[47].

102   Corrections were later applied to the obtained PM6 potentials of mean force (PMFs) by performing geometry op-

103   timizations of the high-level layer models with the exchange correlation functional of 6-31G(d) basis set for

104 B3LYP[43], M06-2X[53] and wB97XD[54], according to Carvalho *et al.* and Bownan *et al.*[55,56]. The coordinates for the-

105 se structures are provided in the SI.

106   Electrostatic embedding[57] was employed and the boundary treated via the link atom approach. Long-range elec-

107 trostatic interactions were described by an adapted implementation of the Particle Mesh Ewald (PME) method for

108 QM/MM[58]. The high-level layer in the reactants complex for AfEST include the **PCL** model compound, S160,

109 the side chains of H285, D255 and G88, G89 and A161. For CalB besides the **PC** and S105, the high-level layer

110 also includes the side chains of H224, D187, the backbone of Q106 and T40 residue. The total number of atoms

111 in the high-level layer in the reactants is 57 for AfEST and 60 for CalB. For the other intermediates, the high-

112 level layer includes the same protein residues plus either the **INT-1**, **EAM**, **INT-2** or the **PC**. The cluster model

113 transition states where also calculated (with the exchange-correlation functional B3LYP) and vibrational frequen-

114 cy calculations were carried out to confirm them. The initial structures were **INT-1** and **INT-2** and the reaction

115 coordinates were restrained in 0.1 Å steps using the umbrella sampling method, except near the transition states

116 were smaller steps of 0.02 Å were employed. The (PMFs) were computed resorting to the Weighted Histogram

117 Analysis Method (WHAM)[59].

118

119 **Results and Discussion**

120 **Catalytic mechanisms of the wild-type enzymes**

121   It is well-known that the enzymes CalB and AfEST display the classical α/β hydrolase fold, dimer arrangement

122 and Ser-His-Asp catalytic triad[60,61] (Figure 1). Yet, they are structurally quite distinct. AfEST has a cap domain

123 composed of five helices from two separate regions (residues 1-54 and 188-246)[39], while CalB lacks this structure

124 and has two highly mobile short α-helixes, helix α5 (residues 142-146) and helix α10 (residues 268-287), where

125 the former acts as the putative lid[40,62]. Furthermore, both enzymes display two pockets, an acyl-binding pocket

126 and a secondary alcohol-binding pocket, with different sizes and orientations[39,40]. The pockets of CalB display a

127 total volume of 204.6 Å^3, while the AfEST pockets have an overall volume of 343.5 Å^3 [63]. The AfEST catalytic

128 triad is composed by the residues S160-H285-D255 and is located at the interface between the classical α/β hy-

129 drolase fold and the cap domain[39]. CalB has the catalytic triad S105-H224-D187, which is located close to the

130 putative lid[40,60,62]. The stated serine residues act as nucleophiles, the histidine residues act as an acid/base (trans-

131 ferring protons between the catalytic serine and the substrate) and are stabilized by the aspartate residues[11,64,65].

132 The enzymes also have a region called oxyanion hole, where a particular spatial arrangement of hydrogen bond

133 donors stabilizes the negative charge that is developed on the oxygen atom of the tetrahedral intermediate struc-

134 tures that are formed during the catalytic mechanism[65,66]. For CalB, the hydrogen bond donors are the backbone

135 amides of T40 and Q106 and the side-chain hydroxyl group of T40[67], while for AfEST the hydrogen bond donors

136 are the backbone amides of G88, G89 and A161[39] (Figure 1).

137
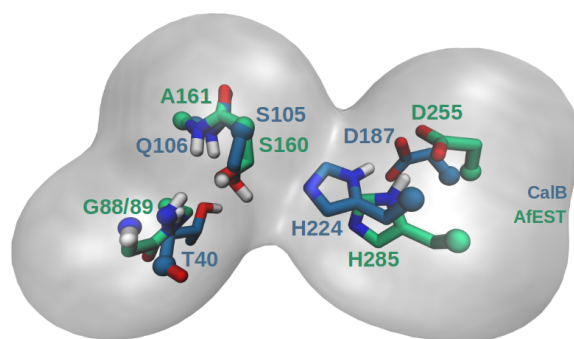
138

139 Figure 1. Catalytic triad and oxyanion hole residues of CalB and AfEST

140

141   The first half part of the catalytic cycle or acylation step (Scheme 1), concerns the nucleophilic attack of the

142 serine side-chain oxygen (O_{Ser}) on the carbonyl carbon of the **ε-Cl** substrate, which occurs concomitantly with

143 proton transfer from the O_{Ser} to the histidine residue forming the first tetrahedral intermediate structure (**INT-1**)[68].

144 In the **INT-1** structure the histidine residue is positively charged and stabilized by the aspartate residue

145   For CalB, the **ε-Cl** substrate binds weakly to its active site pocket as is reflected in the high value of K_M of 0.72

146 M[69]. Accordingly, in the MD simulations we can see that the **ε-Cl** substrate is significantly mobile during the sim-

147 ulations, with the distance between it and the catalytic serine ranging between 3.22 ± 2.30 Å and 9.76 ± 0.81 Å

148 (Figure SI1). Consequently, we resorted to model the **INT-1** as our initial structure, which is in accordance with

149 previous studies[70]. Despite the large distance to the serine residue, we can observe in two replicas, that the car-

150 bonyl oxygen of the **ε-Cl** substrate establishes a hydrogen bond with the side-chain hydroxyl of the oxyanion-

151 hole residue T40 (Figure 2A). The nucleophilic attack proceeds via formation of a first transition state structure

152 (**TS$_1$**), which has a free energy barrier ($\Delta G^{\ddagger}$) of 6.0 ± 0.1 kcal/mol (at the exchange-correlation functional B3LYP

level, Figure 4) generating the **INT-1** (Figure 2B). The **TS$_1$** and all other transition states in this catalytic cycle are concerted, meaning that bond making/breaking events occur simultaneously with proton transfer to or from the histidine. In **INT-1** the backbone amide groups of the oxyanion hole Q106 and T40 stabilize the developing negative charge on the substrate oxygen atom ($O_{oxyanion}$) (1.90 ± 0.12 Å and 2.24 ± 0.32 Å, respectively). This structure has a ΔG of - 1.1 ± 0.1 kcal/mol (with the exchange-correlation functional B3LYP, Figure 4). The HE2 atom of H224 is 1.97 ± 0.24 Å from the oxygen

Scheme 1. First half part mechanism for the CalB and AfEST enzymatic synthesis of PCL.
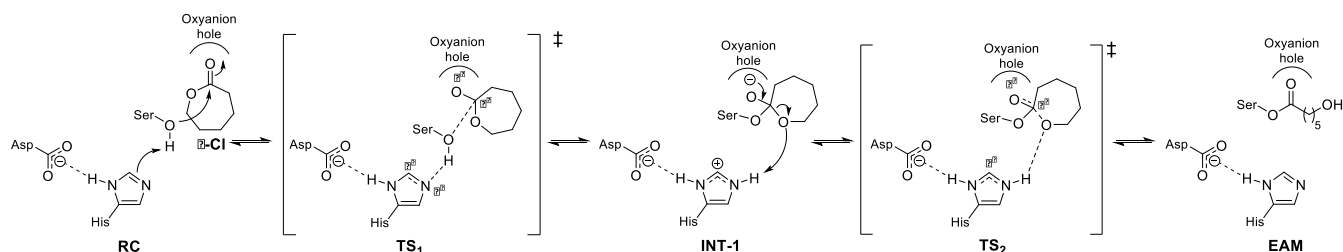
atom of **ε-Cl** substrate (O_{lac}) in the reference structure (Figure 2B).

For the AfEST simulations, we observe less variation in the position of **ε-Cl** substrate (Figure 3A and SI2), which is also in accordance with the reported K_M of 0.093M[37] (7.7 folds lower than the one for CalB). The $O_{oxyanion}$ atom makes a hydrogen bond with the backbone amide group of residue G89 (1.96 ± 0.84 Å, away in the reference structure, Figure 3A). Although the combined size of the pockets is substantially larger in AfEST than in CalB[68], the **ε-Cl** substrate makes more interactions in AfEST because its higher hydrophobic nature[37]. The formation of the **INT-1** from the **RC**, proceeds via the **TS$_1$** with a $\Delta G^{\ddagger}$ of 9.8 ± 0.1 kcal/mol (with the exchange-correlation functional B3LYP, Figure 4B). We also tested the proton transfer step in a stepwise mechanism. In this case the serine proton is transferred to the histidine, while the substrate is not correctly positioned for the nucleophilic attack. The barrier associated with this step amounted to 37 kcal/mol (Figure SI3). In **INT-1**, the HE2 atom is 2.13 ± 0.47 Å from the $O_{lactone}$ atom in the reference structure (Figure 3B) and has a ΔG of 4.4 ± 0.1 kcal/mol (with the exchange-correlation functional B3LYP, Figure 4B). The amide groups of G88, G89 and A161 make hydrogen bonds with the $O_{oxyanion}$ atom (distances of 2.28 ± 0.52 Å, 1.70 ± 0.13 Å and 1.95 ± 0.23 Å, respectively), stabilizing the negative charge that has developed in this atom. Furthermore, the oxygen atoms of D255

7

176   interchangeably make hydrogen bonds with the HD1 atom of the positively charged H285 during the simulations

177   (2.01 ± 0.67 Å, Figure 3B). This interaction highlights the importance of an aspartate residue in the stabilization

178   of the histidine residue.

179   The **INT-1** is then converted into the enzyme activated monomer structure (**EAM**) by ring-opening and assisted

180   by proton transfer from the histidine residue. In CalB, the second transition state structure (**TS$_2$**) is 8.4 ± 0.1

181   kcal/mol above the reactants and the overall $\Delta G^{\ddagger}$ for this step is 9.5 kcal/mol (with the exchange-correlation func-

182   tional B3LYP level, Figure 4A). For AfEST, the **TS$_2$** has an overall $\Delta G^{\ddagger}$ of 19.4 ± 0.2 kcal/mol for the ring-

183   opening (with the exchange-correlation functional B3LYP, Figure 4B).

184
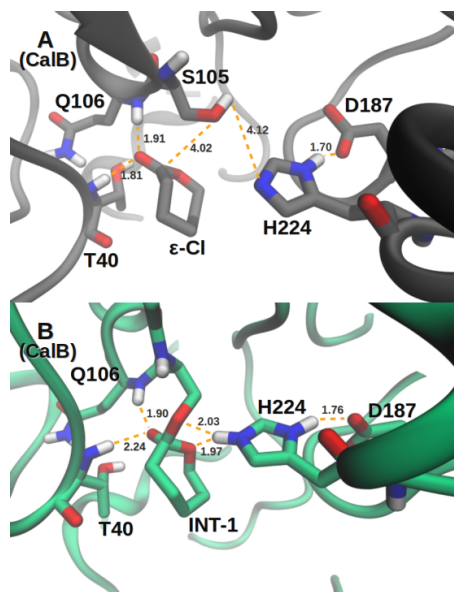
185

186   Figure 2. CalB active site pocket: A) **ε-CL** substrate in the **RC** structure; B) **INT-1** structure.

187

188   For both enzymes the **TS$_2$** show the highest calculated free energy values (including the deacylation steps, that

189   we will detail further in the text). Consequently, the rate-determining step for the enzymatic synthesis of PCL is

190   the formation of the **EAM**, which is in accordance with previous studies[71,72]. For CalB, the reported turnover

191   number (k$_{cat}$) of 72.9 s^{-1} for the immobilized form, corresponds to a free energy of about 15.0 kcal/mol at 45 °C[69].

192   For AfEST, the k$_{cat}$ of 0.064 s^{-1} corresponds to a $\Delta G^{\ddagger}$ of 22.7 kcal/mol at 80°C[37]. Our calculated barriers of 9.5
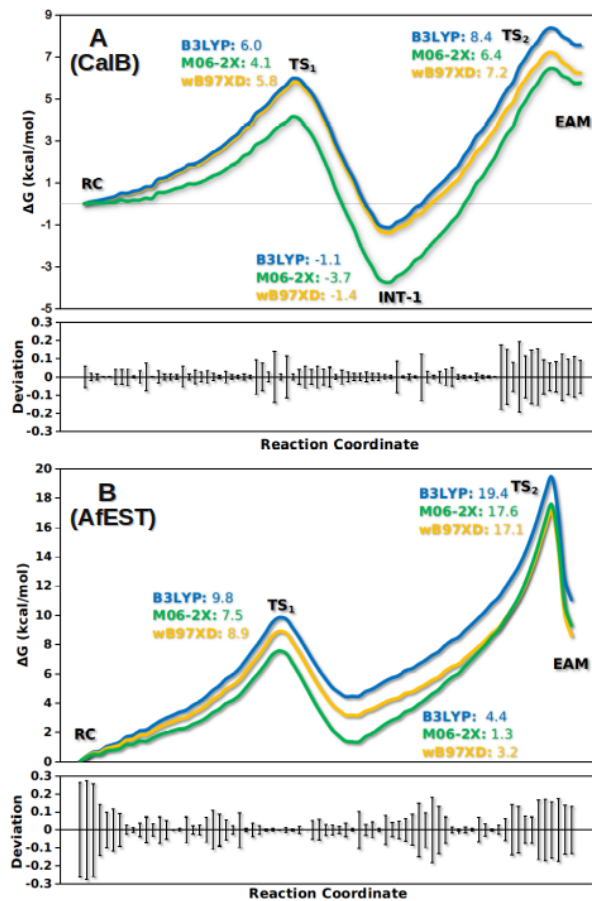
193   kcal/mol and 19.4 ± 0.2 kcal/mol (with the exchange-correlation functional B3LYP for CalB and AfEST - Figure

194   4A and B, respectively) for ring-opening are thus in good agreement with experimental data.

195
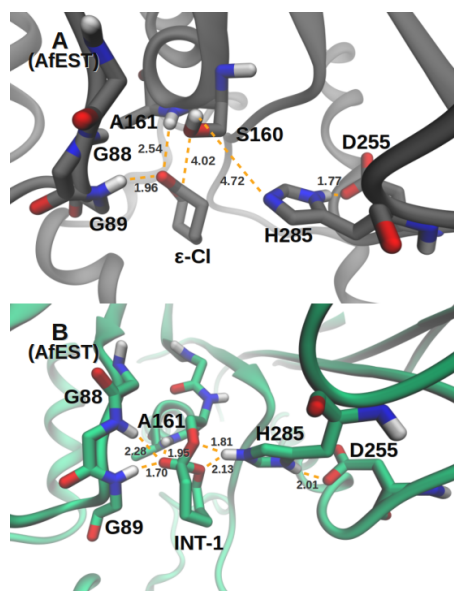
196

197   Figure 3. AfEST active site pocket: A) **ε-Cl** substrate in the **RC** structure; B) **INT-1** structure.

198

Figure 4. Calculated potentials of mean force (PMFs) for the formation of the **EAM** structure (acylation step) with both enzymes. Each line denotes the corrected free energies calculated with different theory levels. More information can be found in Figures SI4 and SI5.

The orientation of the histidine/aspartate residues in the **INT-1** and connected transition states (**TS$_1$** and **TS$_2$**) in the PMFs and in the small cluster models (Figure 2B, Figure 3B and 5) offer an explanation for the enzymes energy differences. As mentioned before, all transition states are concerted, with bond making/breaking events occurring simultaneously with proton transfer to or from the histidine. In the **INT-1** of AfEST, the HE2 atom of the H285 residue is closer to the O_{Ser} atom than to the O_{lac} atom (1.85 Å and 3.42 Å, respectively, Figure 5). This geometry favors coupling of the vibration motions of the proton transfer to O_{Ser} with bond making to the lactone. In fact, **TS$_1$** and **INT-1** are close in energy, favoring the reverse reaction (to **TS$_1$**). In opposition, in CalB the HE2 atom of H224 is closer to the O_{lac} atom than the O_{Ser} atom (1.66 Å and 2.71 Å, respectively, Figure 5). This leads

212 to a latter and higher energy transition state, when going in the reverse direction and much less displacement of

213 the histidine proton in the forward direction (to **EAM**), facilitating concomitant proton transfer and lactone open-

214 ing, decreasing the overall free energy barrier. Consequently, in CalB the active site arrangement is such that it

215 further promotes O_{lac} leaving, lowering the **TS$_2$** barrier. On the other hand, in AfEST, the active site arrangement

216 promotes O_{Ser} leaving, making the **INT-1** to **TS$_1$** backwards free energy barrier lower and the overall $\Delta G^{\ddagger}$ is much

217 higher. To further show this, we ran a simulation in which the histidine residue of CalB is in a position similar to

218 the one observed in AfEST. In this simulation the energy decreases 4.2 ± 0.1 kcal/mol (with the exchange-

219 correlation functional B3LYP level, Figure SI6) as the histidine moves closer to the O_{lac}.

220
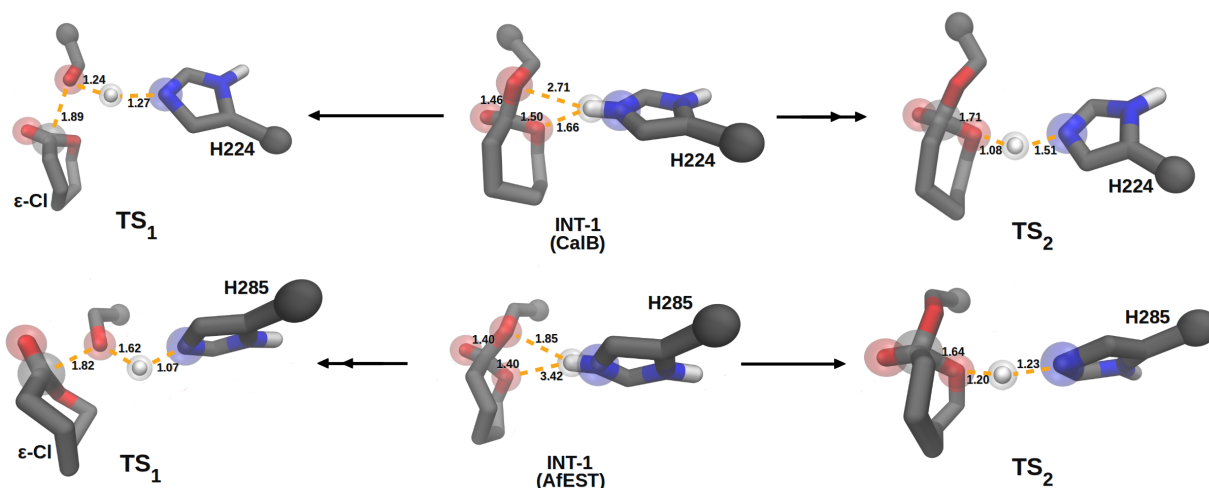
221

222   Figure 5. Scheme of the cluster model structures of **TS$_1$**, **INT-1** and **TS$_2$** for CalB and AfEST (for simplicity in

223 the image representation the oxyanion and catalytic aspartate residues were deleted). The same trend observed in

224 the full models is kept in these small models: In **INT-1** the distance from the histidine proton to O_{lac} is smaller for

225 CalB, favoring the forward reaction, whereas in AfEST the distance to O_{Ser} is smaller. More information can be

226 found in Table SI1. The structures were geometry optimized with the exchange-correlation functional B3LYP

227 with dispersion added.

228

229 **Scheme 2. Second half part mechanism for the CalB and AfEST enzymatic synthesis of PCL.**
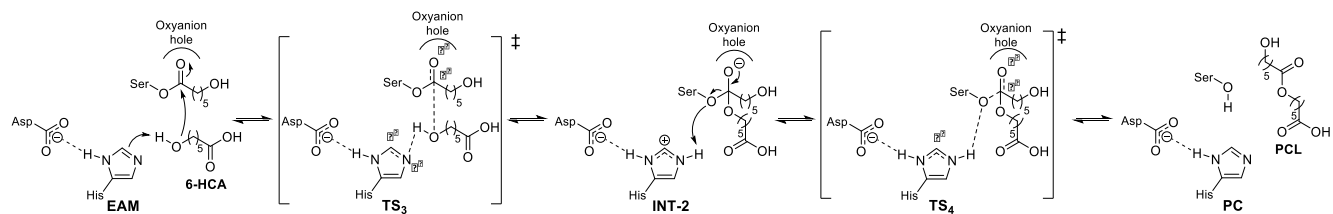
230

231

232   In the second half part of the catalytic cycle (

233   Scheme 2), also called the deacylation step, the second tetrahedral intermediate structure (**INT-2**) is generated

234   after nucleophilic attack by the oxygen atom of the alcohol moiety of a molecule of 6-hydroxycaproic acid (**6-**

235   **HCA**) to the carbonyl carbon atom of the **EAM**. The **6-HCA** molecule is the initiator (init) for the polymerization

236   reaction and was previously formed in a primary step, with the ring-opening of a molecule of **ε-Cl** and post prod-

237   uct hydrolysis[68]. The **PCL** product is formed concomitantly with proton transfer from the histidine to the serine

238   residue, regenerating the free enzyme.

239   In the reaction catalyzed by CalB, the average distance of the carbonyl carbon atom of **EAM** to the hydroxyl

240   oxygen atom of **6-HCA** molecule (O_{init}) is 4.83 ± 0.69 Å and the hydroxyl hydrogen atom of the **6-HCA** mole-

241   cule is 5.06 ± 1.05 Å away from the NE2 atom of H224 Figure 6A and SI7). The **INT-2** is generated via third

242   transition state structure (**TS₃**), which is 7.7 ± 0.2 kcal/mol above the **EAM** (Figure 7A). The hydroxyl hydrogen

243   atom is transferred from the **6-HCA** molecule to the NE2 atom of H224, while in a concerted manner a bond is

244   formed between the O_{init} and the carbonyl carbon of the **EAM**, generating the **INT-2** (1.4 ± 0.1 kcal/mol below

245   the **EAM**, Figure 7A andFigure 6B). The reaction proceeds to the **PCL** product release, through the formation of

246   the last transition state structure (**TS₄**, 4.1 kcal/mol above the **INT-2**, Figure 7A), regenerating the free enzyme

247   that is now, ready for another turnover (Figure 6C).

248   In the reaction catalyzed by AfEST, the **6-HCA** molecule is in the medium pocket and the O_{init} atom of **6-**HCA

249   molecule 4.86 ± 1.61 Å away from carbonyl carbon atom of the **EAM** (Figure 6D and SI8). Bond forming the

250   initiator occurs simultaneously with proton transfer from the HO_{init} atom to H285, as it happens in CalB, with 7.7

251   kcal/mol (with the exchange-correlation functional B3LYP, Figure 7B), being required to reach the **TS₃**. The **INT-**

252   **2** (Figure 6E) is 12.0 kcal/mol below **TS₃** and 7.9 ± 0.1 kcal/mol below the **EAM** (Figure 7B). The **PCL** product

253   is released after breakage of the CO_{Ser} bond and proton transfer from H285 to the serine oxygen (2.09 ± 0.29 Å

12

254   away, Figure 6F). This step requires 7.6 kcal/mol (Figure 7B) and after **PCL** product release, the serine hydroxyl

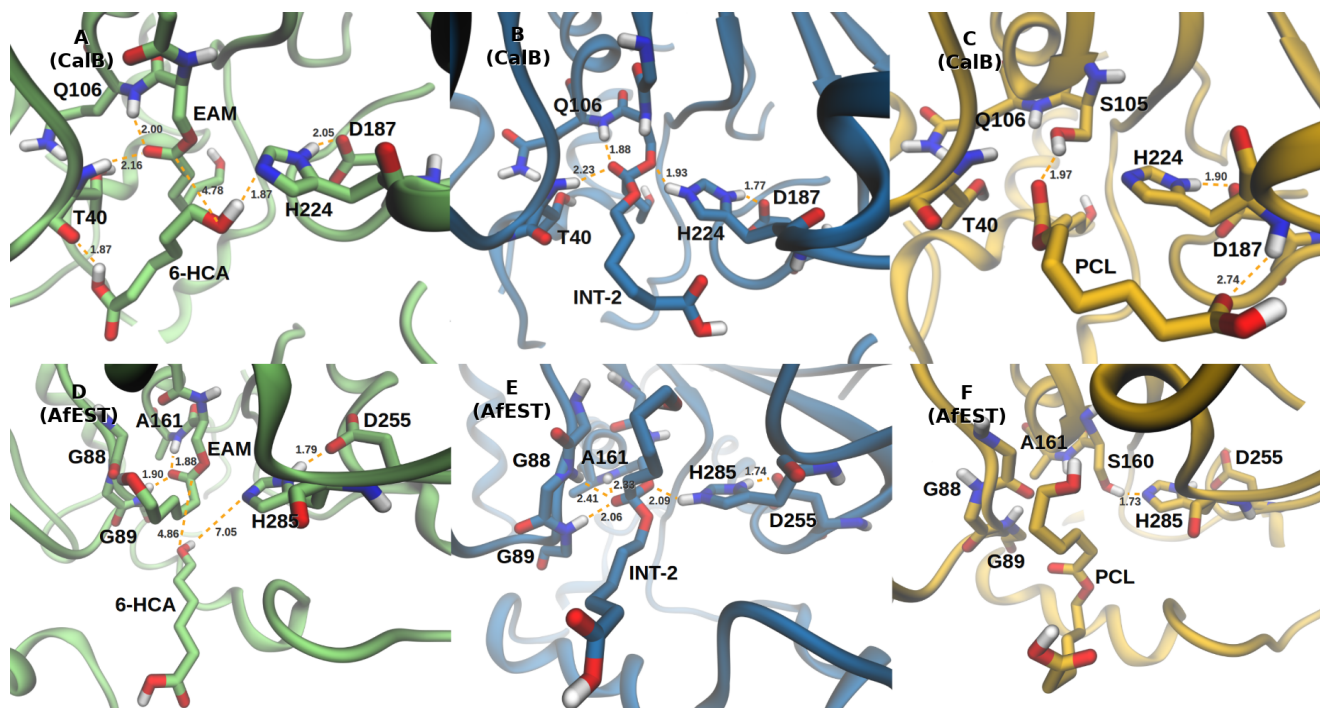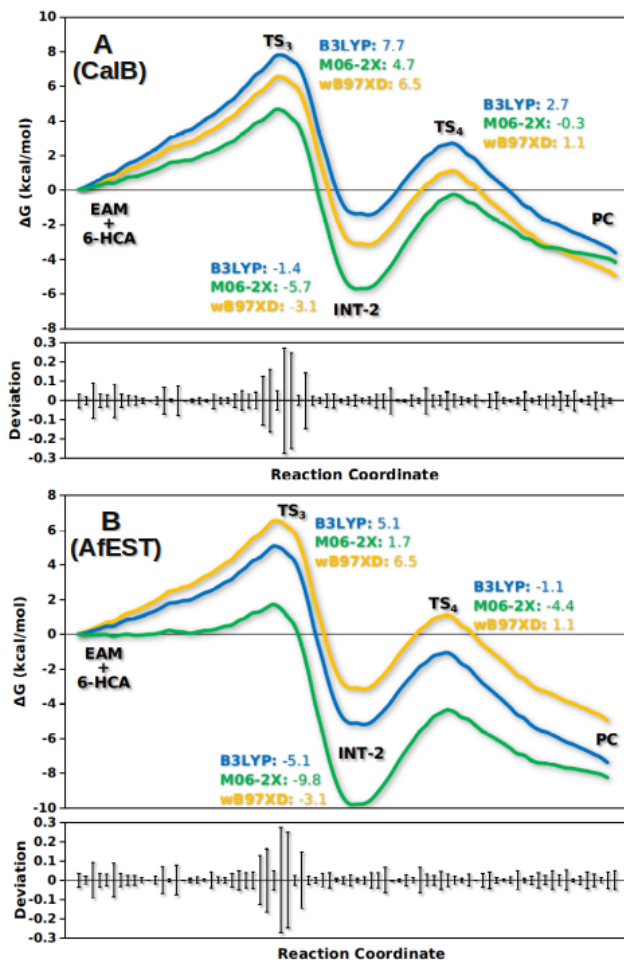255   side-chain is regenerated.

256

257

Figure 6. CalB and AfEST active site pockets, respectively: A and C) **EAM** structure with a **6-HCA** molecule; B and D) **INT-2** structure; C and F) Free enzyme with the **PCL** model compound.

258

Figure 7. Calculated potentials of mean force for the deacylation (**PCL** product release) with both enzymes. Each line denotes the corrected free energies calculated with different theory levels. More information can be found in Figures SI9 and SI10.

4.Conclusions

We have determined the catalytic mechanisms of the wild type CalB and AfEST enzymes by performing QM/MM and MD simulations. By determining the full catalytic cycles, we showed that the formation of the **EAM** is the rate-determining step for this substrate, with the overall barrier for CalB (9.5 kcal/mol) significantly lower than the one for AfEST (19.4 kcal/mol), which is in accordance with the experimental data[37,69,71,72]. Our results also show that the major differences between the enzymes occur exactly during lactone ring opening. By comparing the structures, we can observe that the different scaffolds of the enzymes allow for different arrange-ments of the catalytic triad residues. Here we showed that these different geometries have important consequenc-

14

272 es in the way these enzymes convert **ε-Cl**. Since the transition states are concerted (proton transfer occurs con-

273 comitantly with C-O bond making/breaking), a smaller distance to O_{lac} favors the coupling of the motions of pro-

274 ton transfer to C-O_{lac} bond breaking. In opposition a smaller distance to O_{Ser} favors the coupling of the motions of

275 proton transfer to the C-O_{Ser} bond. In accordance, the histidine in AfEST is significantly closer to O_{Ser} favoring

276 transfer in an early transition state in the reverse direction, while in CalB the same proton is closer to the O_{lac}, re-

277 sulting in the corresponding transition state in the reverse direction and significantly less atom displacement when

278 going in the forward direction leading to a smaller overall free energy barrier.

279   These insights using PCL, as a case-study and CalB and AfEST to mediate esterification reactions, are useful

280 for protein engineering approaches to tailor the enzymes for industrial important poly(esterification), especially

281 those affording biodegradable aliphatic polyesters which are gaining momentum due to the search for more

282 sustainable alternatives, since plastic pollution is endangering the environment.

283 **AUTHOR INFORMATION**

284 **Corresponding Author**

285 *E-mail: atpcarvalho@uc.pt. Website: www.atpcarvalho.pt

286 **Author Contributions**

287 All listed authors have made substantial contributions to this work.

288 ‡ P.F. and B.C.A. contributed equally.

289

290 **Notes**

291 The authors declare no competing financial interest.

292

REFERENCES

(1)   Kobayashi, S.; Makino, A. Enzymatic Polymer Synthesis: An Opportunity for Green Polymer Chemistry. *Chem. Rev.* **2009**, *109* (11), 5288–5353. https://doi.org/10.1021/cr900165z.

(2)   Geyer, R.; Jambeck, J. R.; Law, K. L. Production, Use, and Fate of All Plastics Ever Made. *Science Advances* **2017**, *3* (7), e1700782. https://doi.org/10.1126/sciadv.1700782.

(3)   Vilela, C.; Sousa, A. F.; Fonseca, A. C.; Serra, A. C.; Coelho, J. F. J.; Freire, C. S. R.; Silvestre, A. J. D. The Quest for Sustainable Polyesters – Insights into the Future. *Polym. Chem.* **2014**, *5* (9), 3119–3141. https://doi.org/10.1039/C3PY01213A.

(4)   Vert, M.; Li, S. M.; Spenlehauer, G.; Guerin, P. Bioresorbability and Biocompatibility of Aliphatic Polyesters. *J Mater Sci: Mater Med* **1992**, *3* (6), 432–446. https://doi.org/10.1007/BF00701240.

(5)   Seyednejad, H.; Ghassemi, A. H.; van Nostrum, C. F.; Vermonden, T.; Hennink, W. E. Functional Aliphatic Polyesters for Biomedical and Pharmaceutical Applications. *Journal of Controlled Release* **2011**, *152* (1), 168–176. https://doi.org/10.1016/j.jconrel.2010.12.016.

(6)   Siddiqui, N.; Asawa, S.; Birru, B.; Baadhe, R.; Rao, S. PCL-Based Composite Scaffold Matrices for Tissue Engineering Applications. *Molecular Biotechnology* **2018**, *60* (7), 506–532. https://doi.org/10.1007/s12033-018-0084-5.

(7)   Espinoza, S. M.; Patil, H. I.; San Martin Martinez, E.; Casañas Pimentel, R.; Ige, P. P. Poly-ε-Caprolactone (PCL), a Promising Polymer for Pharmaceutical and Biomedical Applications: Focus on Nanomedicine in Cancer. *International Journal of Polymeric Materials and Polymeric Biomaterials* **2019**, 1–42. https://doi.org/10.1080/00914037.2018.1539990.

(8)   Research, T. M. Polycaprolactone Market to be worth US$ 300 Mn by the end of 2026 - Transparency Market Research http://www.globenewswire.com/news-release/2017/12/04/1220096/0/en/Polycaprolactone-Market-to-be-worth-US-300-Mn-by-the-end-of-2026-Transparency-Market-Research.html (accessed Aug 2, 2019).

(9)   Jérôme, C.; Lecomte, P. Recent Advances in the Synthesis of Aliphatic Polyesters by Ring-Opening Polymerization. *Advanced Drug Delivery Reviews* **2008**, *60* (9), 1056–1076. https://doi.org/10.1016/j.addr.2008.02.008.

(10)   Zhang, J.; Shi, H.; Wu, D.; Xing, Z.; Zhang, A.; Yang, Y.; Li, Q. Recent Developments in Lipase-Catalyzed Synthesis of Polymeric Materials. *Process Biochemistry* **2014**, *49* (5), 797–806. https://doi.org/10.1016/j.procbio.2014.02.006.

(11)   Douka, A.; Vouyiouka, S.; Papaspyridi, L.-M.; Papaspyrides, C. A Review on Enzymatic Polymerization to Produce Polycondensation Polymers: The Case of Aliphatic Polyesters, Polyamides and Polyesteramides. *Progress in Polymer Science* **2017**, *79*. https://doi.org/10.1016/j.progpolymsci.2017.10.001.

(12)   Albertsson, A.-C.; Srivastava, R. K. Recent Developments in Enzyme-Catalyzed Ring-Opening Polymerization. *Advanced Drug Delivery Reviews* **2008**, *60* (9), 1077–1093. https://doi.org/10.1016/j.addr.2008.02.007.

(13)   Yang, Y.; Yu, Y.; Zhang, Y.; Liu, C.; Shi, W.; Li, Q. Lipase/Esterase-Catalyzed Ring-Opening Polymerization: A Green Polyester Synthesis Technique. *Process Biochemistry* **2011**, *46* (10), 1900–1908. https://doi.org/10.1016/j.procbio.2011.07.016.

331   (14)   Shoda, S.; Uyama, H.; Kadokawa, J.; Kimura, S.; Kobayashi, S. Enzymes as Green Catalysts for Precision Macromolecular Synthesis.

332   *Chem. Rev.* **2016**, *116* (4), 2307–2413. https://doi.org/10.1021/acs.chemrev.5b00472.

333   (15)   Zhao, H. Enzymatic Ring-Opening Polymerization (ROP) of Polylactones: Roles of Non-Aqueous Solvents. *Journal of Chemical Tech-*

334   *nology & Biotechnology* **2018**, *93* (1), 9–19. https://doi.org/10.1002/jctb.5444.

335   (16)   Kumar, A.; Gross, R. A. *Candida antartica* Lipase B Catalyzed Polycaprolactone Synthesis: Effects of Organic Media and Tempera-

336   ture. *Biomacromolecules* **2000**, *1* (1), 133–138. https://doi.org/10.1021/bm990510p.

337   (17)   Peeters, J. W.; van Leeuwen, O.; Palmans, A. R. A.; Meijer, E. W. Lipase-Catalyzed Ring-Opening Polymerizations of 4-Substituted ε-

338   Caprolactones: Mechanistic Considerations. *Macromolecules* **2005**, *38* (13), 5587–5592. https://doi.org/10.1021/ma050510j.

339   (18)   Poojari, Y.; Clarson, S. J. Thermal Stability of *Candida antarctica* Lipase B Immobilized on Macroporous Acrylic Resin Particles in

340   Organic Media. *Biocatalysis and Agricultural Biotechnology* **2013**, *2* (1), 7–11. https://doi.org/10.1016/j.bcab.2012.10.002.

341   (19)   Gross, R. A.; Ganesh, M.; Lu, W. Enzyme-Catalysis Breathes New Life into Polyester Condensation Polymerizations. *Trends Biotech-*

342   *nol.* **2010**, *28* (8), 435–443. https://doi.org/10.1016/j.tibtech.2010.05.004.

343   (20)   Poojari, Y.; Beemat, J. S.; Clarson, S. J. Enzymatic Synthesis of Poly(ε-Caprolactone): Thermal Properties, Recovery, and Reuse of Li-

344   pase B from *Candida antarctica* Immobilized on Macroporous Acrylic Resin Particles. *Polymer Bulletin* **2013**, *70* (5), 1543–1552.

345   https://doi.org/10.1007/s00289-013-0916-1.

346   (21)   Polloni, A. E.; Veneral, J. G.; Rebelatto, E. A.; de Oliveira, D.; Oliveira, J. V.; Araújo, P. H. H.; Sayer, C. Enzymatic Ring Opening

347   Polymerization of ω-Pentadecalactone Using Supercritical Carbon Dioxide. *The Journal of Supercritical Fluids* **2017**, *119*, 221–228.

348   https://doi.org/10.1016/j.supflu.2016.09.019.

349   (22)   Zhao, H.; Nathaniel, G. A.; Merenini, P. C. Enzymatic Ring-Opening Polymerization (ROP) of Lactides and Lactone in Ionic Liquids

350   and Organic Solvents: Digging the Controlling Factors. *RSC Adv.* **2017**, *7* (77), 48639–48648. https://doi.org/10.1039/C7RA09038B.

351   (23)   Pellis, A.; Comerford, J. W.; Weinberger, S.; Guebitz, G. M.; Clark, J. H.; Farmer, T. J. Enzymatic Synthesis of Lignin Derivable Pyri-

352   dine Based Polyesters for the Substitution of Petroleum Derived Plastics. *Nature Communications* **2019**, *10* (1), 1762.

353   https://doi.org/10.1038/s41467-019-09817-3.

354   (24)   Yang, J.; Liu, Y.; Liang, X.; Yang, Y.; Li, Q. Enantio-, Regio-, and Chemoselective Lipase-Catalyzed Polymer Synthesis. *Macromo-*

355   *lecular Bioscience* **2018**, *18* (7), 1800131. https://doi.org/10.1002/mabi.201800131.

356   (25)   Champagne, E.; Strandman, S.; Zhu, X.-X. Recent Developments and Optimization of Lipase-Catalyzed Lactone Formation and Ring-

357   Opening   Polymerization   https://onlinelibrary.wiley.com/doi/abs/10.1002/marc.201600494   (accessed   Jul   31,   2019).

358   https://doi.org/10.1002/marc.201600494.

359   (26)   Erhan Ozsagiroglu. Effects of Different Reaction Mediums on Ring Opening Polymerization of Poly(ε-Caprolactone) by Lipase. *African*

360   *Journal of Biotechnology* **2012**, *11* (63). https://doi.org/10.5897/AJB12.1811.

361   (27)   Yang, Y.; Ge, Y.; Zhao, H.; Shi, W.; Li, Q. Lipase-Catalyzed Synthesis of Poly(ε-Caprolactone) and Characterization of Its Solid-State

362   Properties. *Biocatalysis and Biotransformation* **2011**, *29* (6), 337–343. https://doi.org/10.3109/10242422.2011.638057.

363   (28)   Takwa, M.; Wittrup Larsen, M.; Hult, K.; Martinelle, M. Rational Redesign of *Candida antarctica* Lipase B for the Ring Opening

364   Polymerization of d , d -Lactide. *Chemical Communications* **2011**, *47* (26), 7392–7394. https://doi.org/10.1039/C1CC10865D.

365   (29)   Montanier, C. Y.; Chabot, N.; Emond, S.; Guieysse, D.; Remaud-Siméon, M.; Peruch, F.; André, I. Engineering of *Candida antarctica*

366   Lipase B for Poly(ε-Caprolactone) Synthesis. *European Polymer Journal* **2017**, *95*, 809–819. https://doi.org/10.1016/j.eurpolymj.2017.07.029.

367   (30)   Messiha, H. L.; Ahmed, S. T.; Karuppiah, V.; Suardíaz, R.; Ascue Avalos, G. A.; Fey, N.; Yeates, S.; Toogood, H. S.; Mulholland, A. J.;

368 Scrutton, N. S. Biocatalytic Routes to Lactone Monomers for Polymer Production. *Biochemistry* **2018**, *57* (13), 1997–2008.

369 https://doi.org/10.1021/acs.biochem.8b00169.

370   (31)   Levisson, M.; van der Oost, J.; Kengen, S. W. M. Carboxylic Ester Hydrolases from Hyperthermophiles. *Extremophiles* **2009**, *13* (4),

371 567–581. https://doi.org/10.1007/s00792-009-0260-4.

372   (32)   Elleuche, S.; Schröder, C.; Sahm, K.; Antranikian, G. Extremozymes—Biocatalysts with Unique Properties from Extremophilic Micro-

373 organisms. *Current Opinion in Biotechnology* **2014**, *29*, 116–123. https://doi.org/10.1016/j.copbio.2014.04.003.

374   (33)   Sarmiento, F.; Peralta, R.; Blamey, J. M. Cold and Hot Extremozymes: Industrial Relevance and Current Trends. *Front. Bioeng. Bio-*

375 *technol.* **2015**, *3*. https://doi.org/10.3389/fbioe.2015.00148.

376   (34)   Li, Q.; Li, G.; Yu, S.; Zhang, Z.; Ma, F.; Feng, Y. Ring-Opening Polymerization of ε-Caprolactone Catalyzed by a Novel Thermophilic

377 Lipase from *Fervidobacterium nodosum*. *Process Biochemistry* **2011**, *46* (1), 253–257. https://doi.org/10.1016/j.procbio.2010.08.019.

378   (35)   Manco, G.; Giosuè, E.; D'Auria, S.; Herman, P.; Carrea, G.; Rossi, M. Cloning, Overexpression, and Properties of a New Thermophilic

379 and Thermostable Esterase with Sequence Similarity to Hormone-Sensitive Lipase Subfamily from the Archaeon *Archaeoglobus fulgidus*. *Archives*

380 *of Biochemistry and Biophysics* **2000**, *373* (1), 182–192. https://doi.org/10.1006/abbi.1999.1497.

381   (36)   D'Auria, S.; Herman, P.; Lakowicz, J. R.; Bertoli, E.; Tanfani, F.; Rossi, M.; Manco, G. The Thermophilic Esterase from *Archaeoglobus*

382 *fulgidus*: Structure and Conformational Dynamics at High Temperature. *Proteins: Structure, Function, and Bioinformatics* **2000**, *38* (4), 351–360.

383 https://doi.org/10.1002/(SICI)1097-0134(20000301)38:4<351::AID-PROT1>3.0.CO;2-6.

384   (37)   Ma, J.; Li, Q.; Song, B.; Liu, D.; Zheng, B.; Zhang, Z.; Feng, Y. Ring-Opening Polymerization of ε-Caprolactone Catalyzed by a Novel

385 Thermophilic Esterase from the Archaeon *Archaeoglobus fulgidus*. *Journal of Molecular Catalysis B: Enzymatic* **2009**, *56* (2), 151–157.

386 https://doi.org/10.1016/j.molcatb.2008.03.012.

387   (38)   Ren, H.; Xing, Z.; Yang, J.; Jiang, W.; Zhang, G.; Tang, J.; Li, Q. Construction of an Immobilized Thermophilic Esterase on Epoxy

388 Support for Poly(ε-Caprolactone) Synthesis. *Molecules* **2016**, *21* (6). https://doi.org/10.3390/molecules21060796.

389   (39)   De Simone, G.; Menchise, V.; Manco, G.; Mandrich, L.; Sorrentino, N.; Lang, D.; Rossi, M.; Pedone, C. The Crystal Structure of a Hy-

390 per-Thermophilic Carboxylesterase from the Archaeon *Archaeoglobus fulgidus*11Edited by R. Huber. *Journal of Molecular Biology* **2001**, *314* (3),

391 507–518. https://doi.org/10.1006/jmbi.2001.5152.

392   (40)   Stauch, B.; Fisher, S. J.; Cianci, M. Open and Closed States of *Candida antarctica* Lipase B: Protonation and the Mechanism of Interfa-

393 cial Activation. *J. Lipid Res.* **2015**, *56* (12), 2348–2358. https://doi.org/10.1194/jlr.M063388.

394   (41)   Chen, V. B.; Arendall, W. B.; Headd, J. J.; Keedy, D. A.; Immormino, R. M.; Kapral, G. J.; Murray, L. W.; Richardson, J. S.; Richard-

395 son, D. C. MolProbity: All-Atom Structure Validation for Macromolecular Crystallography. *Acta Crystallogr D Biol Crystallogr* **2010**, *66* (Pt 1),

396 12–21. https://doi.org/10.1107/S0907444909042073.

397   (42)   Frisch, M.; Trucks, G.; Schlegel, H.; Scuseria, G.; Robb, M.; Cheeseman, J.; Scalmani, G.; Barone, V.; Mennucci, B.; Petersson, G.; et

398 al. Gaussian 09, Revision B.01. *Gaussian 09, Revision B.01, Gaussian, Inc., Wallingford CT* **2009**.

399   (43)   Ashvar, C. S.; Devlin, F. J.; Bak, K. L.; Taylor, P. R.; Stephens, P. J. Ab Initio Calculation of Vibrational Absorption and Circular Di-

400 chroism Spectra: 6,8-Dioxabicyclo[3.2.1]Octane. *J. Phys. Chem.* **1996**, *100* (22), 9262–9270. https://doi.org/10.1021/jp953738p.

401   (44)   Tomasi, J.; Mennucci, B.; Cammi, R. Quantum Mechanical Continuum Solvation Models. *Chem. Rev.* **2005**, *105* (8), 2999–3094.

402 https://doi.org/10.1021/cr9904009.

(45) Bayly, C. I.; Cieplak, P.; Cornell, W.; Kollman, P. A. A Well-Behaved Electrostatic Potential Based Method Using Charge Restraints for Deriving Atomic Charges: The RESP Model. *J. Phys. Chem.* **1993**, *97* (40), 10269–10280. https://doi.org/10.1021/j100142a004.

(46) Salomon-Ferrer, R.; Case, D. A.; Walker, R. C. An Overview of the Amber Biomolecular Simulation Package: Amber Biomolecular Simulation Package. *Wiley Interdisciplinary Reviews: Computational Molecular Science* **2013**, *3* (2), 198–210. https://doi.org/10.1002/wcms.1121.

(47) Hornak, V.; Abel, R.; Okur, A.; Strockbine, B.; Roitberg, A.; Simmerling, C. Comparison of Multiple AMBER Force Fields and Development of Improved Protein Backbone Parameters. *Proteins* **2006**, *65* (3), 712–725. https://doi.org/10.1002/prot.21123.

(48) Wang, J.; Wolf, R. M.; Caldwell, J. W.; Kollman, P. A.; Case, D. A. Development and Testing of a General Amber Force Field. *J Comput Chem* **2004**, *25* (9), 1157–1174. https://doi.org/10.1002/jcc.20035.

(49) Dourado, D. F. A. R.; Swart, M.; Carvalho, A. T. P. Why the Flavin Adenine Dinucleotide (FAD) Cofactor Needs To Be Covalently Linked to Complex II of the Electron-Transport Chain for the Conversion of FADH2 into FAD. *Chemistry – A European Journal* **2018**, *24* (20), 5246–5252. https://doi.org/10.1002/chem.201704622.

(50) Carvalho, A. T. P.; Barrozo, A.; Doron, D.; Kilshtain, A. V.; Major, D. T.; Kamerlin, S. C. L. Challenges in Computational Studies of Enzyme Structure, Function and Dynamics. *Journal of Molecular Graphics and Modelling* **2014**, *54*, 62–79. https://doi.org/10.1016/j.jmgm.2014.09.003.

(51) Stewart, J. J. P. Optimization of Parameters for Semiempirical Methods V: Modification of NDDO Approximations and Application to 70 Elements. *J Mol Model* **2007**, *13* (12), 1173–1213. https://doi.org/10.1007/s00894-007-0233-4.

(52) Jindal, G.; Warshel, A. Exploring the Dependence of QM/MM Calculations of Enzyme Catalysis on the Size of the QM Region. *J. Phys. Chem. B* **2016**, *120* (37), 9913–9921. https://doi.org/10.1021/acs.jpcb.6b07203.

(53) Zhao, Y.; Truhlar, D. G. The M06 Suite of Density Functionals for Main Group Thermochemistry, Thermochemical Kinetics, Noncovalent Interactions, Excited States, and Transition Elements: Two New Functionals and Systematic Testing of Four M06-Class Functionals and 12 Other Functionals. *Theor Chem Account* **2008**, *120* (1), 215–241. https://doi.org/10.1007/s00214-007-0310-x.

(54) Chai, J.-D.; Head-Gordon, M. Long-Range Corrected Hybrid Density Functionals with Damped Atom-Atom Dispersion Corrections. *Phys Chem Chem Phys* **2008**, *10* (44), 6615–6620. https://doi.org/10.1039/b810189b.

(55) Carvalho, A. T. P.; Dourado, D. F. A. R.; Skvortsov, T.; de Abreu, M.; Ferguson, L. J.; Quinn, D. J.; Moody, T. S.; Huang, M. Catalytic Mechanism of Phenylacetone Monooxygenases for Non-Native Linear Substrates. *Phys Chem Chem Phys* **2017**, *19* (39), 26851–26861. https://doi.org/10.1039/c7cp03640j.

(56) Bowman, A. L.; Grant, I. M.; Mulholland, A. J. QM/MM Simulations Predict a Covalent Intermediate in the Hen Egg White Lysozyme Reaction with Its Natural Substrate. *Chem. Commun. (Camb.)* **2008**, No. 37, 4425–4427. https://doi.org/10.1039/b810099c.

(57) Bakowies, D.; Thiel, W. Hybrid Models for Combined Quantum Mechanical and Molecular Mechanical Approaches. *J. Phys. Chem.* **1996**, *100* (25), 10580–10594. https://doi.org/10.1021/jp9536514.

(58) Nam, K.; Gao, J.; York, D. M. An Efficient Linear-Scaling Ewald Method for Long-Range Electrostatic Interactions in Combined QM/MM Calculations. *J. Chem. Theory Comput.* **2005**, *1* (1), 2–13. https://doi.org/10.1021/ct049941i.

(59) Grossfiled, A. *"WHAM: The Weighted Histogram Analysis Method"*; 2018.

(60) Uppenberg, J.; Hansen, M. T.; Patkar, S.; Jones, T. A. The Sequence, Crystal Structure Determination and Refinement of Two Crystal Forms of Lipase B from *Candida antarctica*. *Structure* **1994**, *2* (4), 293–308. https://doi.org/10.1016/S0969-2126(00)00031-9.

(61) Publishers, B. S. *Protein & Peptide Letters*, 6th ed.; Bentham Science Publishers, 1997; Vol. 4.

439   (62)   Skjøt, M.; De Maria, L.; Chatterjee, R.; Svendsen, A.; Patkar, S. A.; Østergaard, P. R.; Brask, J. Understanding the Plasticity of the α/β

440   Hydrolase Fold: Lid Swapping on the *Candida antarctica* Lipase B Results in Chimeras with Interesting Biocatalytic Properties. *ChemBioChem*

441   **2009**, *10* (3), 520–527. https://doi.org/10.1002/cbic.200800668.

442   (63)   Tian, W.; Chen, C.; Lei, X.; Zhao, J.; Liang, J. CASTp 3.0: Computed Atlas of Surface Topography of Proteins. *Nucleic Acids Res* **2018**,

443   *46* (W1), W363–W367. https://doi.org/10.1093/nar/gky473.

444   (64)   Brady, L.; Brzozowski, A. M.; Derewenda, Z. S.; Dodson, E.; Dodson, G.; Tolley, S.; Turkenburg, J. P.; Christiansen, L.; Huge-Jensen,

445   B.; Norskov, L.; et al. A Serine Protease Triad Forms the Catalytic Centre of a Triacylglycerol Lipase. *Nature* **1990**, *343* (6260), 767.

446   https://doi.org/10.1038/343767a0.

447   (65)   Bezborodov, A. M.; Zagustina, N. A. Lipases in Catalytic Reactions of Organic Chemistry. *Appl Biochem Microbiol* **2014**, *50* (4), 313–

448   337. https://doi.org/10.1134/S0003683814040024.

449   (66)   Simón, L.; Goodman, J. M. Enzyme Catalysis by Hydrogen Bonds: The Balance between Transition State Binding and Substrate Bind-

450   ing in Oxyanion Holes. *J. Org. Chem.* **2010**, *75* (6), 1831–1840. https://doi.org/10.1021/jo901503d.

451   (67)   Raza, S.; Fransson, L.; Hult, K. Enantioselectivity in *Candida antarctica* Lipase B: A Molecular Dynamics Study. *Protein Sci.* **2001**, *10*

452   (2), 329–338. https://doi.org/10.1110/ps.33901.

453   (68)   Almeida, B. C.; Figueiredo, P.; Carvalho, A. T. P. Polycaprolactone Enzymatic Hydrolysis: A Mechanistic Study. *ACS Omega* **2019**, *4*

454   (4), 6769–6774. https://doi.org/10.1021/acsomega.9b00345.

455   (69)   van der Mee, L.; Helmich, F.; de Bruijn, R.; Vekemans, J. A. J. M.; Palmans, A. R. A.; Meijer, E. W. Investigation of Lipase-Catalyzed

456   Ring-Opening Polymerizations of Lactones with Various Ring Sizes: Kinetic Evaluation. *Macromolecules* **2006**, *39* (15), 5021–5027.

457   https://doi.org/10.1021/ma060668j.

458   (70)   Escorcia, A. M.; Sen, K.; Daza, M. C.; Doerr, M.; Thiel, W. Quantum Mechanics/Molecular Mechanics Insights into the Enantioselec-

459   tivity of the O-Acetylation of (R,S)-Propranolol Catalyzed by *Candida antarctica* Lipase B. *ACS Catal.* **2017**, *7* (1), 115–127.

460   https://doi.org/10.1021/acscatal.6b02310.

461   (71)   Kobayashi, S. Enzymatic Ring-Opening Polymerization of Lactones by Lipase Catalyst: Mechanistic Aspects. *Macromolecular Sympo-*

462   *sia* **2006**, *240* (1), 178–185. https://doi.org/10.1002/masy.200650822.

463   (72)   Poojari, Y.; Beemat, J. S.; Clarson, S. J. Enzymatic Synthesis of Poly(ε-Caprolactone): Thermal Properties, Recovery, and Reuse of Li-

464   pase B from *Candida antarctica* Immobilized on Macroporous Acrylic Resin Particles. *Polymer Bulletin* **2013**, *70* (5), 1543–1552.

465   https://doi.org/10.1007/s00289-013-0916-1.

466

467

468

469

470

471

SUPPORTING INFORMATION

Towards sustainable synthesis of polyesters: a QM/MM study of the enzymes CalB and AfEST

Pedro Figueiredo[‡ξ], Beatriz C. Almeida[‡ξ], Daniel F.A.R. Dourado[§], Andreia F. Sousa[†], Armando J. D. Silvestre[†], Alexandra T. P. Carvalho*[ξ]

[ξ] CNC – Center for Neuroscience and Cell Biology, Institute for Interdisciplinary Research (IIIUC), University of Coimbra, 3004-504 Coimbra (Portugal). [‡]These authors contributed equally.
[§] Almac Sciences, Department of Biocatalysis and Isotope Chemistry, Almac House, 20 Seagoe Industrial Estate, Craigavon, BT63 5QD (Northern Ireland UK)
[†] CICECO – Aveiro Institute of Materials, 3810-193 Aveiro (Portugal)
* Email: atpcarvalho@uc.pt; Website: atpcarvalho.com

Contents

513

Material and Methods - Molecular Docking

515 Molecular docking was performed with AutoDock4.2 suite of programs with the Lamarckian Genetic Algorithm (LGA)[1]. A
516 grid box was centered on the oxygen of the side chain of the catalytic serine (residue 160 for AfEST and 105 for CalB). A
517 total of 100 LGA runs were carried out for each ligand-protein complex. The population was 300, the maximum number of
518 generations was 27,000 and the maximum number of energy evaluations was 2,500,000. These initial structures were used to
519 model the **INT-1** and **INT-2** intermediates.
520

Material and Methods - Molecular Dynamics

522 The structures were placed within a pre-equilibrated octahedral box of toluene (a distance of 10.0 Å was set, between the
523 surface of the protein to the box). Counter ions were added to make the entire system neutral. The systems were subjected to
524 two initial energy minimizations and to 500 ps of equilibration in a *NVT* ensemble using Langevin dynamics with small re-
525 straints on the protein (10.0 kcal/mol) to heat the system from 0 K to 300 K. Production simulations were carried out at 300
526 K in the *NPT* ensemble using Langevin dynamics with a collision frequency of 1 ps^{-1}. Constant pressure periodic boundary
527 conditions were imposed with an average pressure of 1 atm. Isotropic position scaling was used to maintain pressure with a
528 relaxation time of 2 ps. The time step was set to 2 fs. SHAKE constraints were applied to all bonds involving hydrogen at-
529 oms[2]. The Particle Mesh Ewald (PME) method[3] was used to calculate electrostatic interactions with a cutoff distance of 10.0
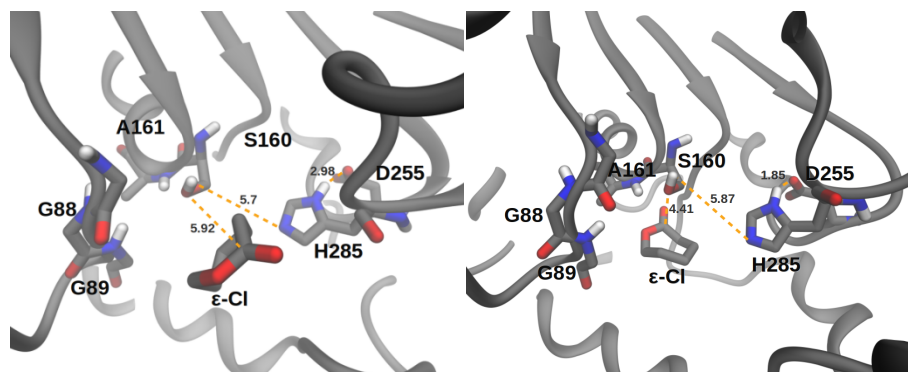530 Å.

531
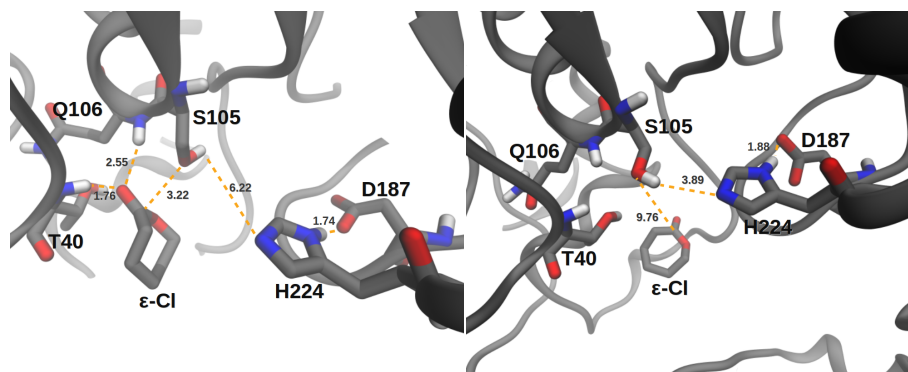
Figure SI8. Representative structures of the MD replicas of CalB RCs.

534

Figure SI9. Representative structures of the MD replicas of AfEST RCs.

(1) Morris, G. M.; Huey, R.; Lindstrom, W.; Sanner, M. F.; Belew, R. K.; Goodsell, D. S.; Olson, A. J. AutoDock4 and AutoDockTools4: Automated docking with selective receptor flexibility. *J. Comput. Chem.* **2009**, 30, 2785–2791.
(2) Ryckaert, J. P.; Ciccotti, G.; Berendsen, H. J. C. Numerical integration of the cartesian equations of motion of a system with constraints: molecular dynamics of n-alkanes. *J. Comput. Phys.* **1977**, 23, 327–341.
(3) Darden, T.; York, D.; Pedersen, L. Particle mesh Ewald: An N-log(N) method for Ewald sums in large systems. *J. Chem. Phys.* **1993**, 98, 10089–10092.
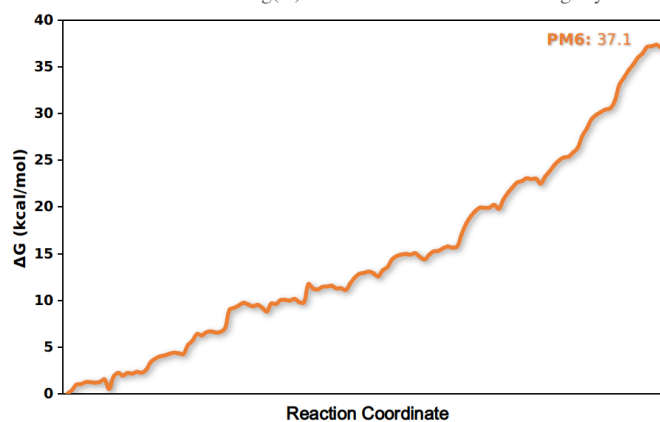
Figure SI3. Proton transfer (PT) for the stepwise mechanism. The much higher free energy barrier for the PT of the stepwise mechanism shows that the concerted mechanism is more feasible.
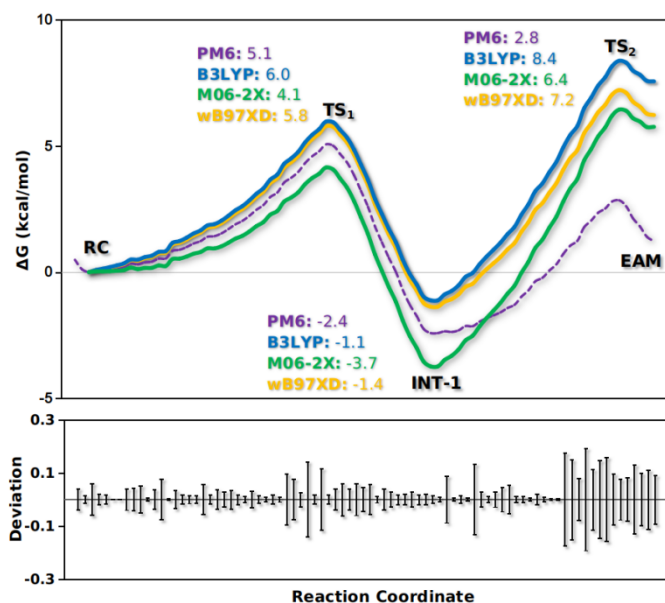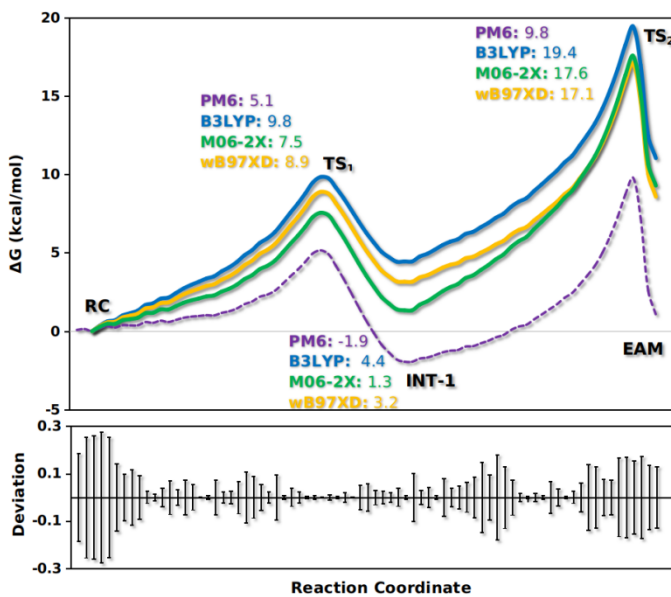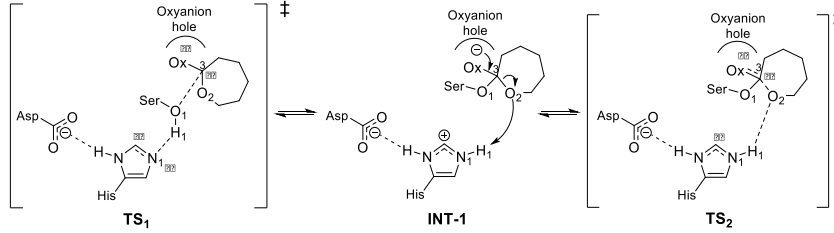
Figure SI4. Calculated potentials of mean force for the acylation step (formation of the EAM structure) in CalB. The dashed line represents the PM6 PMF and the remaining, denotes the corrected free energies calculated with different theory levels.
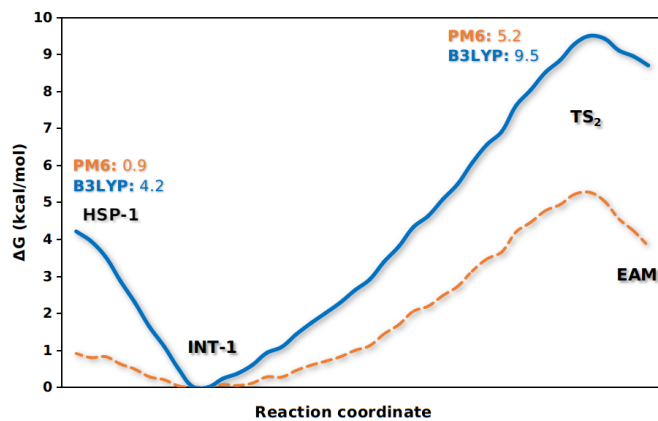
Figure SI5. Calculated potentials of mean force for the acylation step (formation of the EAM structure) in AfEST. The dashed line represents the PM6 PMF and the remaining, denotes the corrected free energies calculated with different theory levels.

563 **Table SI1. Merz Kollman charges for the B3LYP high level layers of structures TS$_1$, INT-1 and TS$_2$ of both**
564   **enzymes.**

565

|		O_{Ser} (O_1)	C_{lact} (C_1)	O_{lact} (O_2)	HE2 (H_1)	N_{Hist} (N_1)	O_{hole} (O_x)
TS1	CaLB	-0.522	0.465	-0.401	0.392	-0.290	-0.390
	AfEST	-0.793	0.737	-0.361	0.674	-0.289	-0.671
INT-1	CaLB	-0.291	0.104	-0.291	0.244	-0.074	-0.648
	AfEST	-0.675	0.746	-0.441	0.359	-0.018	-0.388
TS2	CaLB	-0.322	0.360	-0.355	0.243	0.076	-0.316
	AfEST	-0.513	0.377	-0.320	0.313	-0.083	-0.644

566

567 **Figure SI6. Calculated potential of mean force for the ring-opening reaction (EAM formation) in CalB when the**
568 **histidine residue is in a similar position to the one observed in AfEST. The PMF starts with the histidine residue**
569 **in the latter position (HSP-1), which evolve to the one observed in CalB (INT-1) and ultimately to the EAM**
570 **structure. The dashed line represents the PM6 PMF and the remaining, the correction performed with the**
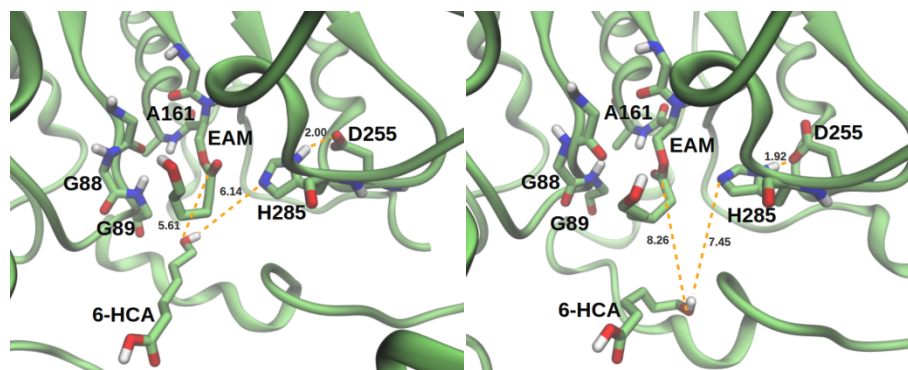571 **B3LYP theory level.**

572

573

574
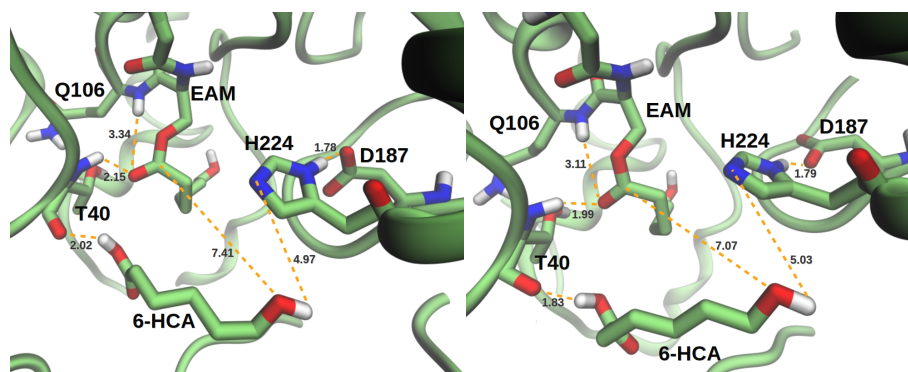
575 **Figure SI7. Representative structures from the MD replicas of the CalBe EAM+6-HCA intermediate.**
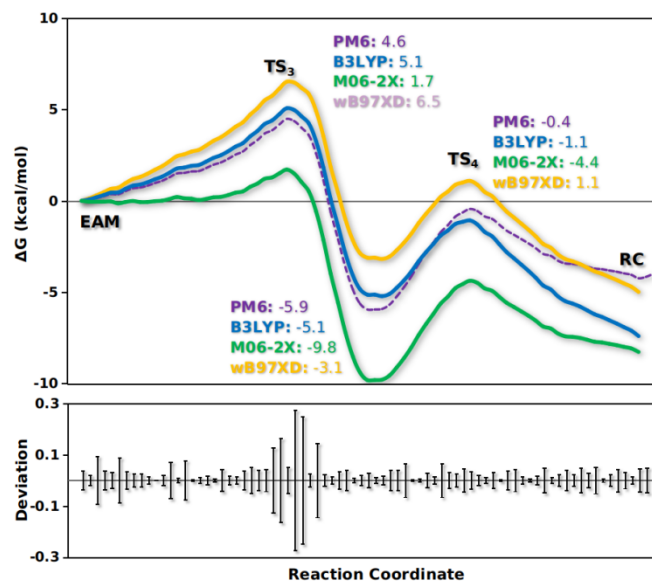
576
577

578

579 **Figure SI8. Representative structures from the MD replicas of the AfEST EAM+ 6-HCA intermediate.**
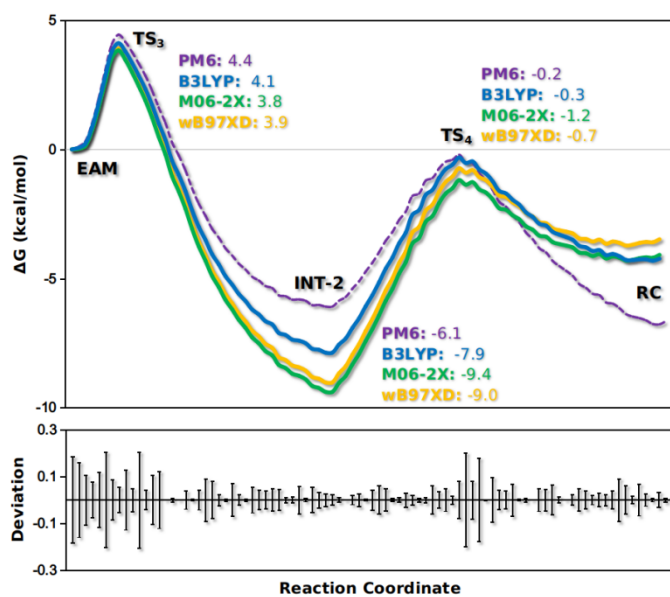
580

26

581

Figure SI9. Calculated potentials of mean force for the deacylation step (formation of the PC structure) in CalB.
The dashed line represents the PM6 PMF and the remaining, denotes the corrected free energies calculated with
different theory levels.

585

586

587

Figure SI10. Calculated potentials of mean force for the deacylation step (formation of the PC structure) in AfEST.
The dashed line represents the PM6 PMF and the remaining, denotes the corrected free energies calculated with
different theory levels.

591